Pattern formation in a complex Swift-Hohenberg equation with phase bistability

Manuel Martínez-Quesada and Germán J. de Valcárcel
Departament d'Òptica, Universitat de València. Dr. Moliner 50 46100 Burjassot, Spain

We study pattern formation in a complex Swift Hohenberg equation with phase-sensitive (parametric) gain. Such an equation serves as a universal order parameter equation describing the onset of spontaneous oscillations in extended systems submitted to a kind of forcing dubbed rocking when the instability is towards long wavelengths. Applications include two-level lasers and photorefractive oscillators. Under rocking, the original continuous phase symmetry of the system is replaced by a discrete one, so that phase bistability emerges. This leads to the spontaneous formation of phase-locked spatial structures like phase domains and dark-ring (phase-) cavity solitons. Stability of the homogeneous solutions is studied and numerical simulations are made covering all the dynamical regimes of the model, which turn out to be very rich. Formal derivations of the rocked complex Swift-Hohenberg equation, using multiple scale techniques, are given for the two-level laser and the photorefractive oscillator

arXiv:1607.02113v2 [nlin.PS] 8 Jul 2016

I. INTRODUCTION

The dynamics of nonlinear systems is largely nontrivial and numerical simulations, involving sophisticated mathematical techniques, usually need to be made to fully understand their temporal evolution. The situation is even more complicated in spatially extended systems, like in nonlinear optics, in which (multi)dimensional variables are present in the dynamics. In these cases an analytical (or semi-analytical) approach that allows us to gain physical insight about the system is only possible if we consider universal models [1], which formally capture the dynamics of nonlinear systems close to critical points (like the threshold of emission in a laser). These models, also known as order parameter equations (OPE) provide a simplified yet powerful description of the system. Their universal character is due to the fact that very different systems (biological, chemical, physical, etc.) are described by the same OPE, the only difference being in the meaning of variables and parameters under this approach.

The symmetries of the system play a central role in the final form of the OPE, those equations are able to capture qualitatively the essential elements of the dynamics. These OPE can be real or complex depending on the fundamental variable (electric field, temperature) that is considered. In nonlinear optics, complex OPE are commonly used since a complex Ginzburg Landau (CGLE) for lasers for finite positive detuning was derived [2] and have proven being very helpful for understanding a variety of systems [3]. Another equation, a complex Swift-Hohenberg (CSHE), which is valid for small detunings (positive and negative) was later obtained [4].

One fundamental symmetry for complex OPE describing spatially extended nonlinear systems is the phase symmetry, as it determines the nature of patterns which are possible in them. In systems with continuous phase symmetry, the dynamics is usually turbulent and the presence of vortices and spiral waves is common. When the systems only allows a finite number of phases (by means a $n:m$ forcing [5] for instance) the dynamics become more ordered and controllable. Furthermore, when a $2:1$ (parametric) forcing is applied to a systems with continuous phase symmetry , the dynamics of the system allows only two phases in it, which leads to the appearance of novel structures in the system like phase domains, domain walls and localized structures (cavity solitons). The proper OPE for the system must reflect this change and a generic equation can be derived for systems with $n:m$ forcing [5]. For parametric forcing a family of OPE, like the parametric complex Ginzburg Landau (PCGLE) [6] are obtained.

Optical systems (like lasers) are usually insensitive to parametric forcing as the nonlinear response of these systems to high frequencies (twice the natural frequency) is negligible. In the last years a novel technique involving a new kind of forcing, known as "rocking" , was introduced [7] . This is a $1:1$ forcing (the frequency of the injection is close to the frequency of the system) so it is appropriate for optical systems. The key factor is that the injection oscillates in time (temporal rocking) [7] or space (spatial rocking) [8] with a given frequency. This modulation modifies the dynamics of the system which becomes phase bistable. It can be shown that a PCGLE describes the universal dynamics of a laser close to threshold under rocking when the undriven system exhibits an homogeneous Hopf bifurcation.

Rocking has been successfully applied (theoretically and experimentally) to a wide range of systems [9]. This has led to the derivation of OPEs describing those systems under certain limits and that provide relevant information of the dynamics. Numerical simulations also prove that the behaviour predicted by these OPEs extends (qualitatively) far beyond the conditions imposed in their derivation, which increases the utility of this universal description. A complex Swift-Hohenberg equation with parametric gain, which describes a photorefractive oscillator (PRO) under the injection of rocking was derived in [10]. Here we show that a very similar equation describes lasers with small detuning when rocking forcing is present, as well as we generalize the result of [10] to more general setups.

The structure of the article is as follows. In section II

we present the equation which is object of our study and obtain their homogeneous solutions. In section III a linear stability analysis is performed to both trivial and homogeneous solutions to study instabilities against perturbations of wavevector k. In section IV we present some numerical simulations of our model for different values of parameters and show the patterns that can be found. We conclude in section V. In the appendices we present the derivation of the equation for lasers and PRO and a comparison with the real Swift-Hohenberg equation.

II. THE MODEL

We consider the spatio-temporal dynamics of extended systems close to a bifurcation to traveling waves of long wavelength, when the system is forced in time close to its natural frequency (1:1 resonance) and uniformly in space. However the type of forcing considered here is not the classic periodic one but has an amplitude which varies on time, specifically whose sign alternates periodically in time. The kind of forcing which we refer to can be thus expressed as:

$$F(t) = P(t)e^{-i\omega_R t} + c.c. \tag{1}$$

where $P(t+T) = P(t)$ is a T-periodic function of time of period $T \ll \frac{2\pi}{\omega_R}$, and ω_R is a high frequency, almost resonant with the natural frequency of the undriven system. A simple realization of $P(t)$ is the function:

$$P(t) = F_0 \cos(\omega t), \tag{2}$$

where $\omega \ll \omega_R$ and F_0 is an amplitude. According to (1) and (2) the forcing phase (sign) alternates in time.

As shown in the Appendices, where two relevant optical systems are analyzed under the action of such forcing, the state of the system can be expressed as:

$$A(\mathbf{r},t) = A_R(t) + \psi(\mathbf{r},t),$$

where $A_R(t)$ is a T-periodic, spatially uniform contribution merely following the forcing, plus a spatially 2-dimensional field $\psi(\mathbf{r},t)$ whose dynamics is governed by the following parametrically driven Swift-Hohenberg equation (written in dimensionless form):

$$\begin{aligned}\partial_t\psi(\mathbf{r},t) &= \mu(1+i\beta)(1-|\psi|^2)\psi + i\alpha\nabla^2\psi \\ &- \left(\Delta - \nabla^2\right)^2\psi - i\theta\psi + \gamma(1+i\beta)(\psi^* - 2\psi).\end{aligned} \tag{3}$$

The first line of this equation contains the usual complex Swift-Hohenberg equation, which models pattern formation arising from a finite wave number instability to traveling waves close to threshold [4, 11–15], whereas in the second line we find the additional terms which appear when rocking is considered [7–10]. The first extra term, $-i\theta\psi$, merely moves the reference frame to the central frequency of the rocking ω_R (see Appendices). The last extra term, $\gamma(1+i\beta)\psi^*$, is the actual novelty as it breaks the phase invariance of the system, which becomes phase bistable as the equation only has the discrete symmetry $\psi \to -\psi$. As for the parameters, μ measures the distance from threshold (it can be removed from the equation by simple scaling but we keep it not to overwhelm the notation), β controls the nonlinear frequency shift of the system, α controls diffraction/dispersion. Other parameters are Δ, the detuning of the cavity from the natural frequency of the unforced system in the optical case, and θ, which is the detuning of the forcing from the natural frequency of the system. Finally the "rocking parameter" γ is proportional to the squared amplitude of rocking F_0^2 and also depends on its frequency ω in a way whose exact form depends on the system considered (see Appendices); note that when $\gamma = 0$ the effect of rocking is lost and (3) becomes a usual complex Swift-Hohenberg equation.

In the following we will take $\beta = 0$ as to not increase the degrees of freedom of the problem without need and also because in the analyzed cases that parameter happens to be zero. On the other hand $\alpha = 1$ in the PRO case, while $\alpha \geq 1$ in the case of laser.

III. PHASE-LOCKED SPATIALLY UNIFORM SOLUTIONS: ROCKED STATES AND THEIR STABILITY

The spatially uniform nontrivial solutions of (3), or "rocked states", can be expressed as $\psi_\pm = |\psi_\pm| e^{i\phi_\pm}$ where:

$$|\psi_\pm|^2 = \mu - 2\gamma - \Delta^2 \pm \sqrt{\gamma^2 - \theta^2} \tag{4a}$$

$$e^{-2i\phi_\pm} = -\frac{i\theta \pm \sqrt{\gamma^2 - \theta^2}}{\gamma}. \tag{4b}$$

The state ψ_- is always unstable as follows from a standard linear stability analysis, so we will not consider it in the following. On the other hand as ϕ_+ can take two values (differing by π) this produces two phase-locked states (with same amplitude) and phase differing by π (bistable phase locking). From now on we rename $\psi_+ \equiv \psi_0$ ($\phi_+ = \phi_0$). The existence of these states requires $\mu - \Delta^2 > 0$ and $\gamma > |\theta|$; see (4a). Moreover, they exist only if $\gamma_0 < \gamma < \gamma_+$, where:

$$\begin{aligned}\gamma_0 &= \begin{cases} |\theta|, \text{ if } |\theta| < (\mu - \Delta^2)/2 \\ \gamma_- \text{ otherwise} \end{cases} \\ \gamma_\pm &= \frac{2(\mu - \theta^2)}{3} \pm \frac{1}{3}\sqrt{(\mu-\theta^2)^2 - 3\Delta^2}.\end{aligned} \tag{5}$$

On the plane $\gamma - \theta$ the existence region is a closed domain ("rocking balloon") as we can see in Fig. 1. Outside that region we have the trivial solution and phase unlocked solutions (traveling waves or patterns).

We have performed a linear stability analysis of the trivial and uniform solutions against perturbations with wavevector k. The eigenvalue with the largest real part

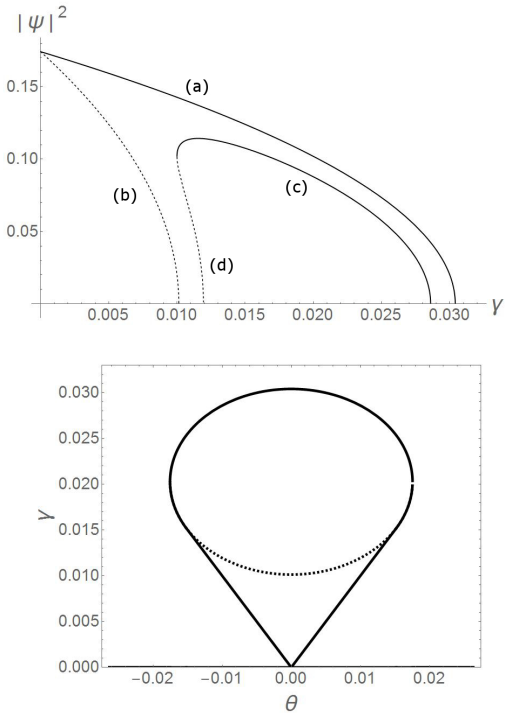

FIG. 1. (Top) Amplitude of the rocking states versus γ for $\theta = 0$, (a) ψ_+ , (b) ψ_- and $\theta = 0.01$, (c) ψ_+ , (d) ψ_- (Bottom) Domain of existence of ψ_+ (bold line) and ψ_- (dotted line) in the $\theta-$ γ plane; the lower bound is the same for both functions.Rest of parameters are $\mu = 0.05$, $\Delta = 0.14$, $\alpha = 2$.

(for the stability of the trivial solution we just set $\psi_0 = 0$) reads:

$$\lambda(k) = \mu - 2\gamma - |\psi_0|^2 - \left(k^2 + \Delta\right)^2 + \sqrt{|\psi_0|^4 - 2\gamma\cos(2\phi_0)|\psi_0|^2 - \left[(\alpha k^2 + \theta)^2 - \gamma^2\right]} \tag{6}$$

As we have two different nonlocal terms in the Swift-Hohenberg (3), $\lambda(k)$ will have, in general, two local maxima. One of them (k_s) is associated with a real eigenvalue and it will give rise to static patterns through a pattern-forming bifurcation; the another one (k_o) corresponds to a complex eigenvalue and it will produce oscillatory solutions (homogeneous or traveling waves) through a Hopf bifurcation from the trivial solution. We could not obtain an exact analytical expression for k_R but an approximated one by considering (as it is observed numerically) that it is close to $-\theta/\alpha$. Writing $k = -\theta/\alpha + \varepsilon$ in (6) and expanding λ to second order in ε, the resulting quadratic expression can be maximized and solved for ε, leading to

$$k_s^2 = \max\left(-\frac{\alpha\theta + 2\Delta S}{\alpha^2 + 2S}, 0\right), \tag{7}$$

where $S = \gamma$ for the trivial solution and $S = \sqrt{\theta^2 + (2\gamma + \Delta^2 - \mu)^2}$ in the case of the rocked states.

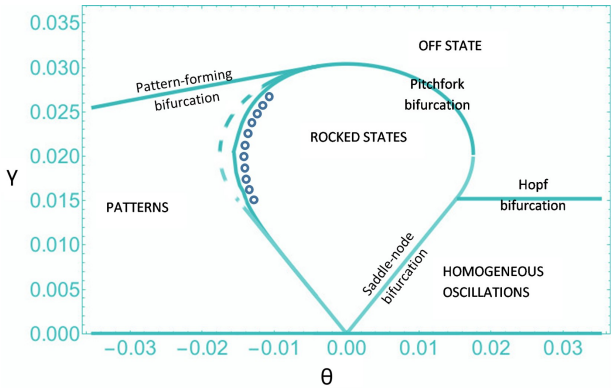

FIG. 2. Bifurcation diagram of equation (3) for $\alpha = 2, \mu = 0.05, \Delta = 0.14$. The dashed line indicates the left boundary of existence of the uniform rocked states, which are become unstable before reaching it. The circles refer to the existence of dark-cavity solitons.

The expression for k_o^2 is just

$$k_o^2 = \max(-\Delta, 0),$$

so for $\Delta > 0$ we will have homogenous oscillations while for $\Delta < 0$ we will obtain traveling waves.

All these results are summarized in Fig. 2 (positive Δ) and Fig. 3 (negative Δ) for $\alpha = 2$ (laser case) and $\mu = 0.05$. For positive Δ, if γ large, the trivial solution, which always exists, is stable. As we decrease the rocking parameter γ, we see bifurcations to other solutions like static patterns (for the trivial state, $k_s^2 > 0 \Longleftrightarrow \theta < -2\gamma\Delta/\alpha$) and homogeneous oscillations (for $\gamma = (\mu - \Delta^2)/2$, $\theta > \gamma$, $k_C^2 = 0$). The transition to uniform rocked states is supercritical in the upper bound (the amplitude ψ_0 becomes 0 along that line). Regarding the lower bound (two straight lines, where $\psi_+ = \psi_-$) there is a saddle-node bifurcation which connects with oscillations by means of a complex eigenvalue for positive θ . For negative θ the rocked states become unstable close to the left edge of the balloon to instabilities (real eigenvalue) of wavenumber k_s^2. In Fig.4 we can see an example of the temporal dynamics of spatially homogenous states close to the bifurcation: as we go closer to this, the period of the oscillations becomes larger and is infinite at the bifurcation.

The analysis for negative Δ is richer, as expected, because in this regime the Swift-Hohenberg equation (3) without rocking ($\gamma = 0$) already displays traveling waves of wavenumber $k_{SH} = \sqrt{-\Delta}$). For large positive θ we still have a Hopf bifurcation connecting trivial and traveling wave solutions (for $\gamma = \mu/2$, $\theta > \sqrt{\mu^2 - 4\Delta^2}/2$, $k_o^2 = -\Delta$). For negative, and small positive θ ($\theta < -2\gamma\Delta/\alpha$) the trivial solution destabilizes to a pattern with leading wavenumber k_s^2 at a certain $\gamma = \gamma(\theta)$. Additionally, for

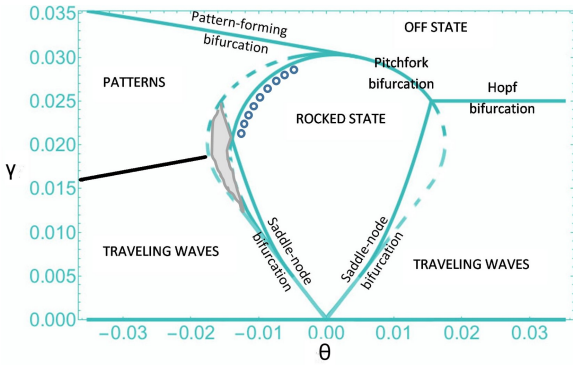

FIG. 3. Bifurcation diagram of equation (3) for $\alpha = 2, \mu = 0.05, \Delta = -0.14$. The dashed line indicates the boundary of existence of the uniform rocked states, which become unstable before reaching it. In the shadowed region the two instabilities (with two different spatial frequencies) for the uniform rocked states are present as explained above. The circles refer to the existence of dark-cavity solitons.

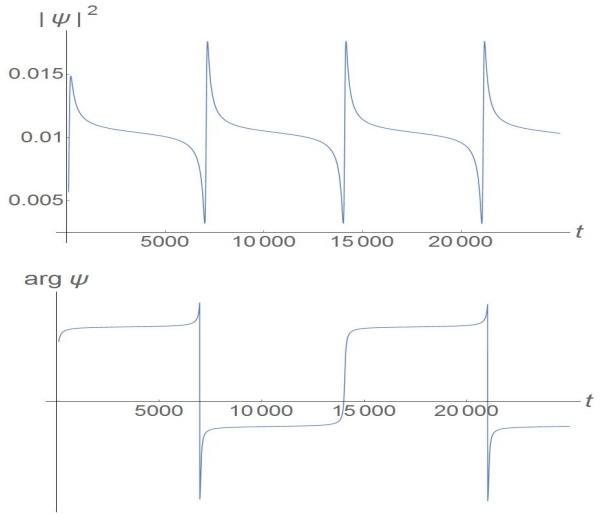

FIG. 4. Temporal evolution of intensity (top) and phase (bottom) of a homogeneous solution close to the saddle-node bifurcation in Fig. 3. Parameters are $\mu = 0.05$, $\Delta = -0.14$, $\alpha = 2$, $\gamma = 0.01$, $\theta = 0.01001$.

small γ we have traveling waves as in the previous case. Regarding the rocked states, these are destabilized in two ways: (i) through a complex eigenvalue with most unstable wavevector $k_o^2 = -\Delta$, which happens symmetrically around θ (see Fig. 3) and (ii) through a real eigenvalue with most unstable wavevector equal to $k^2_{s(rocked)}$, which happens, as in the case of positive detuning, close to the left side of the balloon (here the unstable region is bigger). The presence of these two unstable wavenumbers can be only seen in the simulations in the transient development of the instabilities (Fig. 5) as only one of the two spatial frequencies eventually survives. Close to the lower bound we find (i) and close to the upper bound we

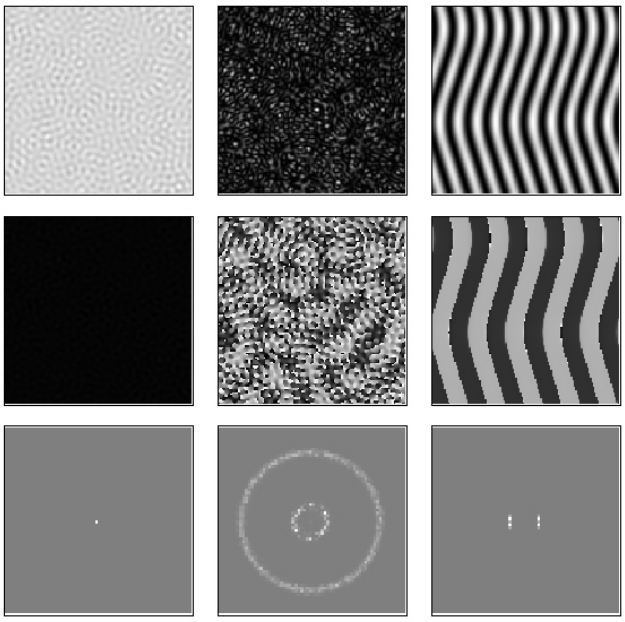

FIG. 5. Competition between two instabilities. Snapshots of intensity (upper row), phase and spatial spectrum (lower row) of the transient dynamics in (left to right) $t = 150$, $t = 1725$ and $t = 120000$. Paremeters are $\mu = 0.05$, $\Delta = -0.14$, $\alpha = 2$, $\gamma = 0.0297$, $\theta = -0.0142$.Size of the windows is 400x400.

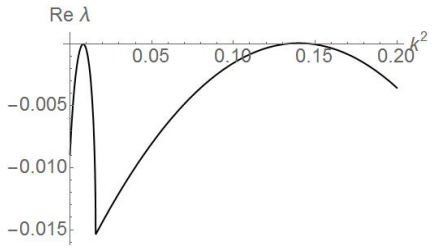

FIG. 6. Real part of the eigenvalue $\lambda(k)$ obtained in the linear stability analysis of the URS solution for parameters: $\mu = 0.05$, $\Delta = -0.14$, $\alpha = 2$, $\gamma = 0.0205$, $\theta = -0.0139$

get (ii). In a range of values of $\Delta(\sim -0.14)$ we find that both instabilities arise simultaneously (the two peaks of $\lambda(k)$ at k_o and $k_{s(rocked)}$ becomes both positive as in Fig. 6: co-dimension-2 point), this happens for a small region in the $\gamma - \theta$ plane (Fig.3). This behaviour also appears (for negative θ) outside of the region where rocked states exist along a line which separates static patterns from traveling waves (Fig. 3).

IV. SPATIAL STRUCTURES

We studied the spatial patterns which appear outside the tongue where rocked (phase-bistable) states exist. In the former case, they basically confirm the previous

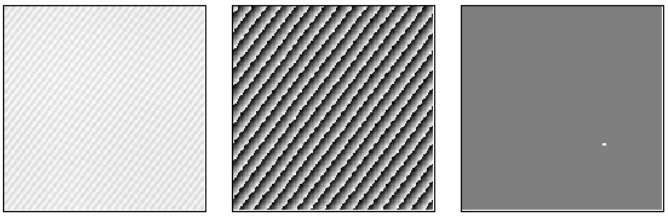

FIG. 7. Intensity (left), phase and spatial spectrum (right) of a traveling wave pattern obtained for $\mu = 0.05$, $\Delta = -0.14$, $\alpha = 2$, $\gamma = 0.012$, $\theta = -0.025$.Size of the windows is 500x500.

analysis as we were able to obtain static spatial patterns which arise from real eigenvalue instabilities, selecting a particular spatial frequency as we have seen in the previous analysis. Then the (slow) dynamics finally leads to a pattern where two spatial modes (of opposite wavenumber) are dominant, leading to roll-like patterns (as in the right column of Fig. 5). Additionally, we observe phase-unlocked patterns as (slightly modulated) traveling waves for negative Δ (Fig. 7), as a result of an instability governed by a complex eigenvalue.

On the other hand, numerical experiments of (3) confirm the existence of a variety of spatial patterns due to the phase bistability and the instabilities studied in the previous section. In the simulations we fix $\alpha = 2$ (remember that $\alpha = 1$ for photorefractive oscillators and $\alpha \geq 1$ for lasers) as it can be shown that, after proper rescaling, the parameter α does not affect the dynamics of the system and its value can be set an arbitrarily. Different values of α just change the temporal scale and the spatial scale associated to the real eigenvalue instability but what is relevant to the dynamics is the ratio between that scale and the one associated to the complex eigenvalue, which is determined by Δ.

Traveling waves (negative Δ) and homogenous oscillations (positive Δ) are found in the phase-unlocked regions. Inside the "rocked" balloon, two uniform rocked states of opposite phase can be connected through domain walls, generating phase domains (Fig. 8). In two spatial dimensions, these domains are always a transient state before one phase dominates [18]. Close (but still inside the stability region) to the edge where the uniform rocked states lose their stability with real eigenvalue (see Section III) the walls become unstable due to curvature effects [18] giving rise to the appearance of labyrinth patterns (Fig. 9). Before reaching the threshold where these labyrinths appear, we find dark-ring cavity solitons [3, 10, 16, 17, 19, 20], which can be written/erased as it is shown in Fig. 10. This happens for both positive and negative Δ.

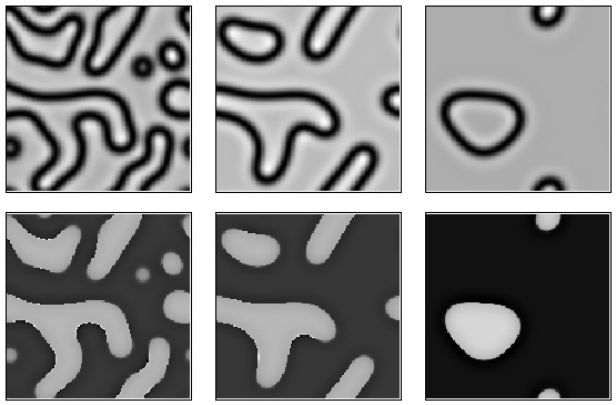

FIG. 8. Contracting phase domains. Snapshots of intensity (upper row), phase(lower row) of transient dynamics of phase domains starting from noise in (left to right) $t = 1000$, $t = 3000$ and $t = 7500$. Paremeters are $\mu = 0.05$, $\Delta = 0.14$, $\alpha = 2$, $\gamma = 0.02$, $\theta = -0.005$.Rest of parameters as in Fig.7

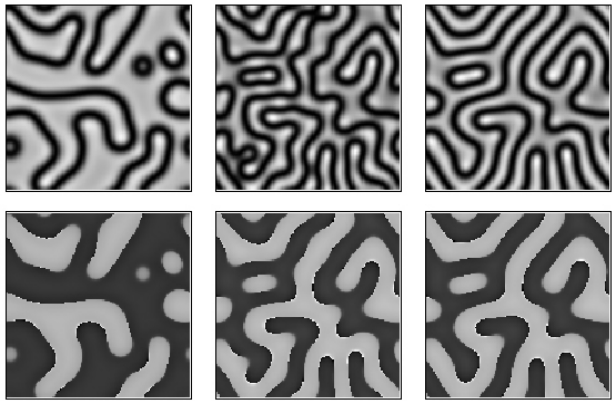

FIG. 9. Labyrinth formation. Snapshots of intensity (upper row), phase(lower row) of transient dynamics of labyrinths starting from left picture in Fig.8 in (left to right) $t = 0$, $t = 500$ and $t = 3000$ for $\theta = -0.012$. Rest of paremeters as in Fig.8

V. CONCLUSIONS

We have proposed and studied, analytically and numerically, a complex Swift-Hohenberg equation with a parametric term that breaks the phase invariance, giving rise to phase-bistable patterns. This equation models diverse nonlinear optical cavities and can be thought of as a universal equation for rocked, spatially extended systems close to a homogeneous Hopf bifurcation. In particular we have derived such an equation for two optical cavities: the two-level laser and the photorefractive oscillator. The structure of the equation, with two nonlocal terms, produces two kinds of instabilities as revealed by a linear stability analysis of the homogeneous states. These

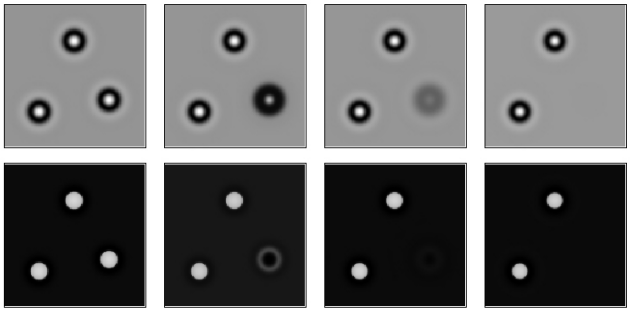

FIG. 10. Writing/Erasing phase cavity solitons. Intensity (upper row) and phase (lower row) plots of transient dynamics of the erasing of a a dark-ring cavity soliton for $\theta = -0.011$. Times (left to right) are $t = 0, t = 150, t = 300, t = 450$. Rest of parameters as in Fig.8

two differ in the character of the eigenvalue governing the instability (real or complex) and in the spatial scale generating a complex variety of spatial patterns, phase locked and phase unlocked. The existence of extended patterns like Ising domain walls and labyrinths is confirmed with numerical solutions as well as of dark-ring (phase) solitons.

APPENDIX A: LASER

Our starting point is the set of Maxwell-Boch Equations with a bichromatical injected signal [9]:

$$\begin{aligned} \partial_t E &= \sigma\left[1-(1+i\Delta)E+P\right]+i\nabla^2 E+F\cos(\omega t)e^{i\theta t} \\ \partial_t P &= -(1-i\Delta)P+(r-N)E \\ \partial_t N &= b\left[-N+\frac{1}{2}\left(E^*P+P^*E\right)\right] \end{aligned} \tag{8}$$

The complex fields E and P are the scaled envelopes of the electric field and polarization, $-N$ is proportional to the difference between the population inversion and its steady value in the absence of lasing. $\sigma = \kappa/\gamma_\perp$ and $b = \gamma_\parallel/\gamma_\perp$, where κ, $\gamma_\perp$, and $\gamma_\parallel$ are, respectively, the decay rates of E, P, and N. The transverse Laplacian $\nabla^2 = \partial_x^2 + \partial_y^2$, where the spatial coordinates (x, y) have been normalized so as to make unity the diffraction coefficient, and $t = \gamma_\perp T$ where T is the physical time. r is the pump parameter and the detuning $\Delta = (\omega_C - \omega_A)/(\gamma_\perp + \kappa)$, being ω_C (ω_A) the cavity (atomic) frequency.

Eqs. (8) have been written in the frequency frame $\omega_0 = (\gamma_\perp\omega_C + \kappa\omega_A)/(\gamma_\perp + \kappa)$ of the on-axis, or plane-wave $\left(\nabla^2 E = 0\right)$, lasing solution in the absence of injected signal. In particular, this means that the actual injected field at the entrance face of the amplifying medium, $\mathcal{E}_{in}$, is of the form:

$$\mathcal{E}_{in} = E_{in}\exp\left(-i\omega_0 T\right) + c.c. \tag{9}$$

$$= E_{in}\exp\left(-i\omega_0\gamma_\perp^{-1}t\right) + c.c. \tag{10}$$

We will consider two types of scales: Fast and slow.

Fast Scales

Regarding the scales, we will consider that the detuning Δ and laplacian ∇^2 are $\mathcal{O}(\varepsilon)$ .As we consider class C lasers, σ and b are $\mathcal{O}\left(\varepsilon^0\right)$. Additionally, $F = \mathcal{O}\left(\varepsilon^2\right)$ and $\theta = \mathcal{O}(\varepsilon)$. Time scales are $T_1 = \varepsilon t$ and $T_2 = \varepsilon^2 t$, the pump is $r = 1 + \varepsilon^2 r_2$ (we are close to the threshold). The variables will be written in the form:

$$(E, P, N) = (E_0, P_0, N_0) + \varepsilon(E_1, P_1, N_1) + \varepsilon^2(E_2, P_2, N_2) + ... \tag{11}$$

$\mathcal{O}\left(\varepsilon^0\right)$

At this order $E_0 = P_0 = N_0 = 0$.

$\mathcal{O}(\varepsilon)$

This is the first nontrivial order and reads:

$$N_1 = 0, \tag{12}$$

$$\mathcal{L}_0\left|v_1\right\rangle = 0, \tag{13}$$

where

$$\mathcal{L}_0 = \begin{pmatrix} -\sigma & \sigma \\ r_0 & -1 \end{pmatrix},$$

and we have introduced the notation

$$\left|v_i\right\rangle = \begin{pmatrix} E_i \\ P_i \end{pmatrix}, \quad i = 1, 2, 3, \ldots \tag{14}$$

Eq. (13) can be easily solved with the help of the left eigenvectors of matrix $\mathcal{L}_0$:

$$\left\langle\zeta_1\right|\mathcal{L}_0 = 0\left\langle\zeta_1\right|, \quad \left\langle\zeta_2\right|\mathcal{L}_0 = \mu\left\langle\zeta_2\right| \tag{15}$$

$$\left\langle\zeta_1\right| = (1, \sigma), \tag{16}$$

$$\left\langle\zeta_2\right| = (1, -1), \quad \mu = -(1+\sigma). \tag{17}$$

Projecting Eq. (13) onto $\langle\zeta_1|$ we obtain $0 = 0$, and projecting onto $\langle\zeta_2|$ we obtain

$$P_1 = E_1, \tag{18}$$

hence

$$\left|v_1\right\rangle = E_1\begin{pmatrix} 1 \\ 1 \end{pmatrix}. \tag{19}$$

$\mathcal{O}\left(\varepsilon^2\right)$

Making use of Eqs. () and (), we obtain

$$N_2 = |E_1|^2 , \tag{20}$$

$$\frac{\partial}{\partial T_1}|v_1\rangle = \mathcal{L}_0|v_2\rangle + |g_2\rangle . \tag{21}$$

where

$$|g_2\rangle = \begin{pmatrix} i\nabla^2 E_1 - i\sigma\Delta E_1 + F_1\cos(\omega T_1)\, e^{i\theta T_2} \\ i\Delta E_1 \end{pmatrix} \tag{22}$$

Projecting Eq. (21) onto $\langle\zeta_1|$ and making use of Eq. (18) we obtain

$$(\sigma+1)\frac{\partial E_1}{\partial T_1} = i\nabla^2 E_1 + F_1\cos(\omega T_1)\, e^{i\theta T_2}. \tag{23}$$

We solve

$$E_1(\overrightarrow{x}, T_1, T_2) = A_1(\overrightarrow{x}, T_1, T_2) + F_1(T_1, T_2) \tag{24}$$

$$F_1(T_1, T_2) \equiv \frac{F}{\omega}\sin(\omega T_1)\, e^{i\theta T_2} \tag{25}$$

$$(\sigma+1)\frac{\partial A_1}{\partial T_1} = i\nabla^2 A_1 \tag{26}$$

Projecting onto $\langle\zeta_2|$ and making use of Eq. (23) we obtain

$$P_2 = -\left(\frac{\partial}{\partial T_1} - i\Delta\right)E_1 + (1+\sigma)E_2, \tag{27}$$

$\mathcal{O}\left(\varepsilon^3\right)$

$$\frac{\partial}{\partial T_1}|v_2\rangle + \frac{\partial}{\partial T_2}|v_1\rangle = \mathcal{L}_0|v_3\rangle + |g_3\rangle \tag{28}$$

where

$$|g_3\rangle = \begin{pmatrix} 0 \\ \left(r_2 - |E_1|^2\right)E_1 + i\Delta P_2 \end{pmatrix}$$

Projecting

$$\sigma\left(\frac{\partial}{\partial T_1} - i\Delta\right)\left[\left(\frac{\partial}{\partial T_1} - i\Delta\right)E_1 + (1+\sigma)E_2\right] =$$
$$-(1+\sigma)\frac{\partial E_1}{\partial T_2} + \sigma\left(r_2 - |E_1|^2\right)E_1 \tag{29}$$

We can rewrite this as following

$$\sigma\left(\frac{\partial}{\partial T_1} - i\Delta\right)(1+\sigma)E_2 = g(T_1, T_2)$$

where

$$g(T_1,T_2) = -\sigma\left(\frac{\partial}{\partial T_1} - i\Delta\right)^2 A_1 - (1+\sigma)\frac{\partial A_1}{\partial T_2}$$
$$+\sigma\left(r_2 - |A_1|^2\right)A_1 + -\sigma\left(\frac{\partial}{\partial T_1} - i\Delta\right)^2 F_1$$
$$-(1+\sigma)\frac{\partial F_1}{\partial T_2} + \sigma\left(r_2 - |F_1|^2\right)F_1 - 2\sigma|A_1|^2 F_1$$
$$-2\sigma|F_1|^2 A_1 - \sigma F_1^2 A_1^* + \sigma F_1^* A_1^2 \tag{30}$$

The solution can be written formally as:

$$E_2 = \frac{1}{\sigma(1+\sigma)}\left(e^{i\Delta T_1} + \int_0^{T_1} g(T_1, T_2)\, dT_1 + A_2(T_2)\right)$$

To ensure convergence it must be true that:

$$\lim_{T_1\to\infty}\frac{1}{T_1}\int_0^{T_1} g(T_1, T_2)\, dT_1 = 0 \tag{31}$$

Taking into account that if A_1 is homogeneous then it does not depend on T_1 the following condition must be fulfilled (we make use of (26)):

$$(1+\sigma)\frac{\partial A_1}{\partial T_2} = -\sigma\left(\frac{i\nabla^2}{1+\sigma} - i\Delta\right)^2 A_1 \tag{32}$$
$$+\sigma\left(r_2 - |A_1|^2\right)A_1 - \sigma\left(\frac{F}{\omega}\right)^2 A_1 - \frac{\sigma}{2}\left(\frac{F}{\omega}\right)^2 e^{2i\theta T_2} A_1^*$$

in order to avoid divergences (in the case $\nabla^2 A_1 = 0$)
We finally compute the time derivative $\partial_t A_1 = \left(\varepsilon\frac{\partial}{\partial T_1} + \varepsilon^2\frac{\partial}{\partial T_2}\right)(\varepsilon A_1)$ up to third order in ε which, making use of (32) and (26), setting $\psi = e^{-i\theta T_2}A_1$ and rescaling to the original variables, we obtain:

$$(1+\sigma)\frac{\partial\psi}{\partial t} = \sigma\left(\frac{i\nabla^2}{1+\sigma} - i\Delta\right)^2\psi - (1+\sigma)i\theta\psi +$$
$$i\nabla^2\psi + \sigma\left(r - 1 - |\psi|^2\right)\psi - 2\gamma\psi + \gamma\psi^* \tag{33}$$
$$\text{where } \gamma = \frac{1}{2}\frac{F^2\sigma}{(1+\sigma)^2\omega^2}$$

Slow Scales

The scales in this case will be:

$$r = r_0 + \varepsilon^2 r_2$$
$$r_0 = 1 + \Delta^2\varepsilon^2 \qquad \Delta \sim O(\varepsilon)$$
$$\omega \sim O(\varepsilon^2) \quad F \sim O(\varepsilon^3)$$
$$(E, N, P) \sim (E_1, P_1, N_1)\varepsilon + (E_2, P_2, N_2)\varepsilon^2 + ... \tag{34}$$

$O(\varepsilon)$

$$N_1 = 0 \tag{35}$$
$$L_0|v_1\rangle = 0$$

$$L_0 = \begin{pmatrix} -\sigma & \sigma \\ 1 & -1 \end{pmatrix} \tag{36}$$

The left-eigenvectors are $\langle\xi_1| = (1,\sigma)$ and $\langle\xi_1| = (1,-1)$ with eigenvalues 0 and $-(1+\sigma)$ respectively. We can use this to write:

$$\langle\xi_1| L_0 |v_1\rangle = 0 \langle\xi_1| v_1\rangle$$
$$\langle\xi_2| L_0 |v_1\rangle = -(1+\sigma) \langle\xi_2| v_1\rangle$$
$$v_1 = \begin{pmatrix} E_1 \\ P_1 \end{pmatrix} \tag{37}$$

We obtain $E_1 = P_1$
$O(\varepsilon^2)$

$$N_2 = |E_1|^2 \tag{38}$$
$$\frac{\partial}{\partial T_1}|v_1\rangle = L_0|v_2\rangle + |g_2\rangle$$

$$|g_2\rangle = \begin{pmatrix} i\nabla^2 E_1 - i\sigma\Delta E_1 \\ i\Delta E_1 \end{pmatrix} \tag{39}$$

Using the same procedure as above, we obtain (if we set $E_2 = 0$):

$$(1+\sigma)\frac{\partial E_1}{\partial T_1} = i\nabla^2 E_1 \tag{40}$$
$$P_2 = -\frac{i}{(1+\sigma)}\left(\nabla^2 E_1 - (1+\sigma)\Delta E_1\right) \tag{41}$$

$O(\varepsilon^3)$

$$\frac{\partial}{\partial T_1}|v_2\rangle + \frac{\partial}{\partial T_2}|v_1\rangle = L_0|v_3\rangle + |g_3\rangle \tag{42}$$
$$|g_3\rangle = \begin{pmatrix} F\cos(\omega T_1)\, e^{i\theta T_2} \\ (r_2 - |E_1|^2 E_1 + i\Delta P_2 \end{pmatrix} \tag{43}$$

Now we obtain the following equation:

$$\sigma\left(\frac{\partial}{\partial T_1} - i\Delta\right)P_2 = -(1+\sigma)\frac{\partial E_1}{\partial T_2} +$$
$$F\cos(\omega T_1)\, e^{i\theta T_2} + \sigma(r_2 - |E_1|^2)E_1 \tag{44}$$

Using (41) and undoing the scaling:

$$\frac{\partial E}{\partial t} = \frac{\partial E_1}{\partial T_1}\varepsilon + \frac{\partial E_1}{\partial T_2}\varepsilon^2 \tag{45}$$

We can write:

$$(1+\sigma)\frac{\partial E}{\partial t} = \sigma\left(\frac{i\nabla^2}{1+\sigma} - i\Delta\right)^2 E + i\nabla^2 E +$$
$$\sigma\left(r - 1 - |E|^2\right)E + F\cos(\omega t)\, e^{i\theta t} \tag{46}$$

Setting $E \equiv Ae^{-i\theta t}$ the previous equation becomes

$$(1+\sigma)\frac{\partial A}{\partial t} = \sigma\left(\frac{i\nabla^2}{1+\sigma} - i\Delta\right)^2 A - (1+\sigma)i\theta A +$$
$$i\nabla^2 A + \sigma\left(r - 1 - |A|^2\right)A + F\cos(\omega t) \tag{47}$$

If the frequency ω is high compared with the dynamics of the system we can set: $T = \omega t \to \varepsilon^{-1}t$ with $T \gg t$ and as it is done in [7] separate the slow dynamics from the fast dynamics:
Specifically $t = \varepsilon^{-1}T + \tau$

$$A(\tau, T) = A_0(\tau, T) + \varepsilon A_1(\tau, T) \tag{48}$$

No we solve at different orders
$O(\varepsilon^{-1})$

$$(1+\sigma)\frac{\partial A_0}{\partial T} = F\cos(T) \to A_0(T) = \frac{F}{(1+\sigma)\omega}\sin(T) + i\psi(\tau) \tag{49}$$

$O(\varepsilon^0)$
The equation reads at this order:

$$(1+\sigma)\frac{\partial A_1}{\partial T} + (1+\sigma)\frac{\partial \psi}{\partial \tau} =$$
$$\sigma\left(\frac{i\nabla^2}{1+\sigma} - i\Delta\right)^2 A_0 + (1+\sigma)i\theta A_0 + i\nabla^2 A_0$$
$$+\sigma\left(r - 1 - |A_0|^2\right)A_0 + F\cos(T) \tag{50}$$

This can be written as $(1+\sigma)\frac{\partial A_1(\tau,T)}{\partial T} = g(T,\tau)$ which can be solved: $A_1(\tau,T) = (1+\sigma)^{-1}\int_0^T dT' g(T',\tau) + B(\tau)$. The boundness of this requires:

$$\lim \frac{1}{T}\int_0^T dT' g(T',\tau) = 0 \tag{51}$$

Therein, we obtain the following solvability condition:

$$(1+\sigma)\frac{\partial \psi}{\partial t} = \sigma\left(\frac{i\nabla^2}{1+\sigma} - i\Delta\right)^2 \psi - (1+\sigma)i\theta\psi +$$
$$i\nabla^2\psi + \sigma\left(r - 1 - |\psi|^2\right)\psi - 2\gamma\psi + \gamma\psi^* \tag{52}$$
$$\text{where } \gamma = \frac{1}{2}\frac{F^2\sigma}{(1+\sigma)^2\omega^2}$$

This condition is exactly the same equation as 33,so we recover the result that we obtained considering fast scales by just assuming that F and ω are large. So, independently of the set of scales we consider, the final equation is consistent.
Setting $\frac{\nabla^2}{1+\sigma} \equiv \nabla'^2$, $\tau \equiv \frac{\sigma}{\sigma+1}t$, $\theta' \equiv \frac{\sigma+1}{\sigma}\theta$, $\gamma' \equiv \frac{\gamma}{\sigma}$, $\alpha \equiv \frac{\sigma+1}{\sigma}$ and defining $\mu = r - 1$ we can write (removing the commas for simplicity):

$$\partial_t\psi = (\mu - 2\gamma - i\theta)\psi - |\psi|^2\psi - \left(\Delta - \nabla^2\right)^2\psi + i\alpha\nabla^2\psi + \gamma\psi^* \tag{53}$$

APPENDIX B: PRO

Our starting point is the set of equations as in [10] in which we consider a bichromatical injection and we make the change $(E', N') \longrightarrow (E, N)e^{i\Delta t}$ for convenience. After removing the commas, we get:

$$\sigma^{-1}\partial_t E = -(1+i\Delta)E + i\nabla^2 E + N + F\cos(\omega t)e^{i\theta t} \tag{54}$$

$$\partial_t N = -(1-i\Delta)N + g\frac{E}{1+|E|^2}$$

where $E(\mathbf{r},t)$ is the slowly varying envelope of the intracavity field, $N(\mathbf{r},t)$ is the complex amplitude of the photorefractive nonlinear grating, $\mathbf{r}$=(x,y) are the transverse coordinates, $\nabla^2 = \partial_x^2 + \partial_y^2, \sigma = \kappa_P \tau$ is the product of the cavity linewidth κ_P with the photorefractive response time τ ($\sigma \gtrsim 10^8$ under typical conditions, and $\tau \sim 1$ s), t is time measured in units of τ, the detuning $(\omega_C - \omega_P)/\kappa_P$ (ω_P and ω_C are the frequencies of the pump and its nearest longitudinal mode, respectively), g is the (real) gain parameter that depends of the crystal parameters and the geometry of the interaction.

The scales will be $\sigma \sim O(\varepsilon^{-4})$ (results are independent of the specific scale provided that σ very large) and $\Delta, \theta \sim O(\varepsilon)$, which implies $\nabla^2 \sim O(\varepsilon)$. We also assume that g is close to threshold, $g = 1 + g_2\varepsilon^2$ and that $F \sim O(\varepsilon), \omega \sim O(1)$. We will have "two times" , fast and slow: $t = T_1 + \varepsilon^{-1}T_2$ so that $\partial_t = \partial_{T_1} + \varepsilon\partial_{T_2}$.We also set:

$$(E, N) = (E_0, N_0) + \varepsilon(E_1, N_1) + \varepsilon^2(E_2, N_2) + ... \tag{55}$$

$$F = \varepsilon F_1 \cos(\omega T_1)e^{i\theta T_2} \tag{56}$$

Now we will solve the previous equations (54) at different orders. At order $O(1)$ we trivially have $E_0 = N_0 = 0$.

$O(\varepsilon)$

$$\begin{aligned} &0 = -E_1 + N_1 + F_1\cos(\omega T_1)e^{i\theta T_2} \\ &\partial_{T_1} N_1 = -N_1 + E_1 \end{aligned} \tag{57}$$

The solution is

$$\begin{aligned} N_1 &= E_1 - F_1\cos(\omega T_1)e^{i\theta T_2} \\ E_1 &= F_1\cos(\omega T_1)e^{i\theta T_2} + F_1/\omega\sin(\omega T_1)e^{i\theta T_2} \\ &+\varphi_1(\mathbf{r}, T_2) \equiv E_1^\omega + \varphi_1 \end{aligned}$$

$O(\varepsilon^2)$

$$\begin{aligned} &0 = -E_2 + (-i\Delta + i\nabla^2)E_1 + N_2 \\ &\partial_{T_1} N_2 + \partial_{T_2} N_1 = -N_2 + i\Delta N_1 + E_2 \end{aligned} \tag{58}$$

We solve

$$\begin{aligned} &N_2 = E_2 - (-i\Delta + i\nabla^2)E_1 \\ &E_2 = \int_0^{T_1} G_2(T_1, T_2)dT_1 + \varphi_2(\overrightarrow{x}, T_2) \equiv E_2^\omega + \varphi_2 \\ &G_2(T_1, T_2) = (-i\Delta)(-F_1\omega\cos(\omega T_1)e^{i\theta T_2} + \\ &F_1\cos(\omega T_1)e^{i\theta T_2} + F_1\cos(\omega T_1)e^{i\theta T_2}) \\ &+(i\theta)F_1/\omega\sin(\omega T_1)e^{i\theta T_2} - \partial_{T_2}\varphi_1 + i\nabla^2\varphi_1 \end{aligned} \tag{59}$$

Solvability of E_2 requires:

$$\lim_{T_1\to\infty}\frac{1}{T_1}\int_0^{T_1} G_2(T_1, T_2)dT_1 = 0 \tag{60}$$

The oscillatory terms in (59) vanish so the previous condition remains:

$$\partial_{T_2}\varphi_1 = i\nabla^2\varphi_1 \tag{61}$$

$O(\varepsilon^3)$

$$\begin{aligned} &0 = -E_3 + (-i\Delta + i\nabla^2)E_2 + N_3 \\ &\partial_{T_1} N_3 + \partial_{T_2} N_2 = -N_3 + i\Delta N_2 + \\ &E_3 + (g-1)E_1 + |E_1|^2 E_1 \end{aligned} \tag{62}$$

We already know that

$$\begin{aligned} E_1 &= E_1^\omega(T_1, T_2) + \varphi_1(\mathbf{r}, T_2) \\ E_2 &= E_2^\omega(T_1, T_2) + \varphi_2(\mathbf{r}, T_2) \end{aligned} \tag{63}$$

We solve:

$$N_3 = E_3 - (-i\Delta + i\nabla^2)E_2 \tag{64}$$

$$E_3 = \int_0^{T_1} G_3(T_1, T_2)dT_1 + \varphi_3(\mathbf{r}, T_2) \tag{65}$$

$$\begin{aligned} &G_3(T_1, T_2) = \\ &\left[(-i\Delta)(\partial_{T_1}E_2^\omega + \partial_{T_2}E_1^\omega) + (g_2 - 1 - \Delta^2)E_1^\omega - \partial_{T_2}E_2^\omega\right] + \\ &\left[-\partial_{T_2}\varphi_2 + (g_2-1)\varphi_1 - (-i\Delta + i\nabla^2)^2\varphi_1 + i\nabla^2\varphi_2 - |\varphi_1|^2\varphi_1\right] \\ &\left[|E_1^\omega|^2 E_1^\omega + 2E_1^\omega|\varphi_1|^2 + (E_1^\omega)^*\varphi_1^2 + 2|E_1^\omega|^2\varphi_1 + |E_1^\omega|^2\varphi_1^*\right] \end{aligned} \tag{66}$$

Solvability of E_3 requires:

$$\lim_{T_1\to\infty}\frac{1}{T_1}\int_0^{T_1} G_3(T_1, T_2)dT_1 = 0 \tag{67}$$

The oscillatory terms in (66) vanish so the previous condition remains:

$$\begin{aligned} \partial_{T_2}\varphi_2 = &-(-i\Delta + i\nabla^2)^2\varphi_2 + i\nabla^2\varphi_2 - \\ &|\varphi_1|^2\varphi_1 - 2\gamma\varphi_1 - \gamma\varphi_1^* e^{i2\theta T_2} \end{aligned} \tag{68}$$

where $\gamma = \frac{1}{2}\frac{F^2}{\omega^2}(\omega^2+1)$
Finally, developing up to second order we have

$$\begin{aligned} &E = \varepsilon E_1 + \varepsilon^2 E_2 \\ &N = \varepsilon N_1 + \varepsilon^2 N_2 = \\ &\varepsilon(E_1 - F_1\cos(\omega T_1)e^{i\theta T_2}) + \varepsilon^2(E_2 - (-i\Delta + i\nabla^2)E_1) = \\ &(1 + (-i\Delta + i\nabla^2))E - F\cos(\omega t)e^{i\theta t} \\ &\varphi = \varepsilon\varphi_1 + \varepsilon^2\varphi_2 \qquad \partial_t\varphi = \varepsilon\partial_{T_2}\varphi_1 + \varepsilon^2\partial_{T_2}\varphi_2 \end{aligned} \tag{69}$$

Undoing the scaling and if we make the change $\psi = i\varphi e^{i\theta T_2}$, we can write (defining $\mu = g - 1$):

$$\partial_t\psi = (\mu - 2\gamma - i\theta)\psi - |\psi|^2\psi + i\nabla^2\psi - \left(\nabla^2 - \Delta\right)^2\psi + \gamma\psi^* \tag{70}$$

[1] M.C. Cross and P.C. Hohenberg, Rev. Mod. Phys. **65**, 851 (1993).
[2] P. Coullet, L. Gil, and F. Rocca, Opt. Commun. **73**, 403 (1989).
[3] K. Staliunas and V. J. Sánchez-Morcillo, *Transverse Patterns in Nonlinear Optical Resonators* (Springer, Berlin, 2003).
[4] J. Lega, J. V. Moloney, and A. C. Newell, Phys. Rev. Lett. **73**, 2978 (1994).
[5] P. Coullet and K. Emilsson, Physica D **61**, 119 (1992).
[6] P. Coullet et al. Phys. Rev. Lett. **65** 1352 (1990).
[7] G. J. de Valcárcel and K. Staliunas, Phys. Rev. E **67,** 026604 (2003).
[8] G. J. de Valcárcel and K. Staliunas, Phys. Rev. Lett. **105,** 054101 (2010).
[9] G. J. de Valcárcel, Manuel Martínez-Quesada, and K. Staliunas, Phil. Trans. R. Soc. A, **372** 20140008 (2014)
[10] A. Esteban-Martin et al. Phys Rev. Lett. **94** 223903 (2005).
[11] K. Staliunas, Phys. Rev. A **48** 1573 (1993).
[12] K. Staliunas, M. F. H. Tarroja, G. Slekys, C. O. Weiss, and L. Dambly, Phys. Rev. A **51**, 4140 (1995).
[13] S. Longhi and A. Geraci, Phys. Rev. A **54**, 4581 (1996).
[14] S. Longhi, Opt. Commun. **149**, 335 (1998).
[15] V. J. Sánchez-Morcillo, E. Roldán, G. J. de Valcárcel, and K. Staliunas, Phys. Rev. A **56**, 3237 (1997).
[16] K. Staliunas and Víctor J. Sánchez Morcillo, Phys. Lett. A **241**, 28-34 (1998).
[17] Víctor J. Sánchez Morcillo and K. Staliunas, Phys. Rev. E **60** 6153 (1999).
[18] R. Gallego, Maxi San Miguel and Raúl Toral, Phys. Rev. E **61** 2241 (2000).
[19] D. Gomila, P. Colet, G-L Oppo and M. San Miguel, Phys. Rev. Lett. **87** 194101 (2001).
[20] V. B. Taranenko, K. Staliunas and C. O. Weiss , Phys. Rev. Lett. **81** 2236 (1998).